UNCLASSIFIED
SECURITY CLASSIFICATION OF THIS PAGE

REPORT DOCUMENTATION PAGE

Form Approved
OMB No 0704-0188
Exp Date Jun 30, 1986

1a REPORT SECURITY CLASSIFICATION UNCLASSIFIED	1b RESTRICTIVE MARKINGS
2a SECURITY CLASSIFICATION AUTHORITY	3 DISTRIBUTION / AVAILABILITY OF REPORT Approved for public release; distribution unlimited.
2b DECLASSIFICATION / DOWNGRADING SCHEDULE	
4 PERFORMING ORGANIZATION REPORT NUMBER(S) HDL-TR-2148	5 MONITORING ORGANIZATION REPORT NUMBER(S)
6a NAME OF PERFORMING ORGANIZATION Harry Diamond Laboratories 6b OFFICE SYMBOL (If applicable) SLCHD-ST-AP	7a NAME OF MONITORING ORGANIZATION
6c ADDRESS (City, State, and ZIP Code) 2800 Powder Mill Road Adelphi, MD 20783-1197	7b ADDRESS (City, State, and ZIP Code)
8a NAME OF FUNDING / SPONSORING ORGANIZATION Center for Night Vision & Electro-Optics 8b OFFICE SYMBOL (If applicable)	9 PROCUREMENT INSTRUMENT IDENTIFICATION NUMBER
8c ADDRESS (City, State, and ZIP Code) Ft Belvoir, VA 22060	10 SOURCE OF FUNDING NUMBERS PROGRAM ELEMENT NO: P61210.H2511 / PROJECT NO: AH25 / TASK NO / WORK UNIT ACCESSION NO

11 TITLE (Include Security Classification)
Preparation, Structure, and Spectroscoptic Properties of Nd^{3+}:$\{La_{1-x}Lu_x\}_3[Lu_{1-y}Ga_y]_2(Ga)_3O_{12}$ Crystals

12 PERSONAL AUTHOR(S)
See reverse

13a TYPE OF REPORT	13b TIME COVERED	14 DATE OF REPORT (Year, Month, Day)	15 PAGE COUNT
Final	FROM Feb 87 TO Nov 87	August 1988	

16 SUPPLEMENTARY NOTATION
AMS code: 612120.H2500; HDL project: 520851

17 COSATI CODES		
FIELD	GROUP	SUB-GROUP
20	02	
20	05	

18 SUBJECT TERMS (Continue on reverse if necessary and identify by block number)
Neodymium, crystal-field theory, rare earth, spectra

19 ABSTRACT (Continue on reverse if necessary and identify by block number)

Single crystals of lanthanum lutetium gallium garnet (LLGG) were grown by the Czochralski pulling technique. X-ray diffraction and elemental analysis performed on these samples indicate that these garnets do not form with simple stoichiometry described as $\{La\}_3^{\prime}[Lu]_2^{\prime}(Ga)_3O_{12}^{\prime}$ but with increased Lu concentration in the dodecahedral site and Ga occupancy in the octahedral site. Optical absorption and fluorescence spectra confirm these results, showing inhomogeneous broadening of the spectral lines of Nd^{3+}. Various laser gain measurements were performed on $\{La_{1-x}Lu_x\}_3[Lu_{1-y}Ga_y]_2(Ga)_3O_{12}$ crystals containing 4.3 and 1.2 atomic percent Nd^{3+} to determine the usefulness of this material as a laser. No optical gain was observed. To ascertain why, time-resolved, site-selection spectroscopy measurements were made to determine the effects of ion/ion interaction, and two-photon excitation spectroscopy measurements were made to determine the effects of excited state absorption. The results show the presence of very weak energy transfer between ions in nonequivalent crystal-field sites and the presence of very strong two-photon absorption transitions.

20 DISTRIBUTION / AVAILABILITY OF ABSTRACT	21 ABSTRACT SECURITY CLASSIFICATION
☒ UNCLASSIFIED/UNLIMITED ☐ SAME AS RPT ☐ DTIC USERS	UNCLASSIFIED
22a NAME OF RESPONSIBLE INDIVIDUAL Clyde A. Morrison	22b TELEPHONE (Include Area Code) (202) 394-2042 22c OFFICE SYMBOL SLCHD-ST-AP

DD FORM 1473, 84 MAR 83 APR edition may be used until exhausted
All other editions are obsolete

SECURITY CLASSIFICATION OF THIS PAGE
UNCLASSIFIED

12. PERSONAL AUTHOR(s) (cont'd)

Toomas H. Allik, Susan A. Stewart—Science Applications International Corporation;
Dhiraj K. Sardar,* Gregory J. Quarles, Richard C. Powell—Oklahoma State University;
Clyde A. Morrison, Gregory A. Turner—Harry Diamond Laboratories;
Milan R. Kokta—Union Carbide Corporation; and
Wayne W. Hovis and Albert A. Pinto—Center for Night Vision and Electro-Optics

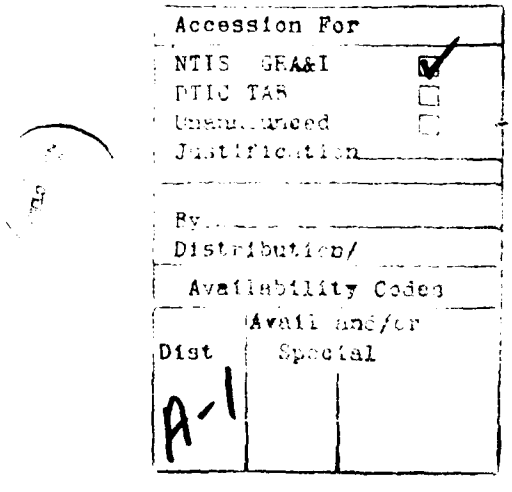

*Permanent address: Division of Earth and Physical Sciences, University of Texas at San Antonio.

CONTENTS

FIGURES

FIGURES (cont'd)

TABLES

1. INTRODUCTION

Although Nd-doped $Y_3Al_5O_{12}$ (YAG)* has become a standard laser material, there is still significant interest in characterizing the properties of other types of Nd-doped materials that can be pumped with GaAlAs laser diodes emitting radiation at 800 ± 20 nm. The spectral emission of laser diodes at 800 nm is resonant with the $^4F_{3/2}$ and $^2H_{9/2}$ Nd^{3+} absorption bands. The advantage derived from the spectral match leads to a reduction of the amount of heat that is deposited in the medium, thus reducing the thermomechanical requirements of the laser host. With the commercial availability of single laser diodes with powers exceeding 1 W and two-dimensional arrays producing 4.0 kW/cm^2, it is useful to determine if other materials can be found with spectral and thermo-optic properties leading to improved laser characteristics. Desirable properties of new laser-diode-pumped solid-state lasers include a longer fluorescence lifetime, a broader absorption band, and a higher absorption coefficient than Nd:YAG. We report here the results of x-ray diffraction, elemental and spectroscopic analysis, and gain measurements obtained on Nd^{3+}-doped $\{La_{1-x}Lu_x\}_3[Lu_{1-y}Ga_y]_2(Ga)_3O_{12}$ (lanthanum lutetium gallium garnet--LLGG) crystals.

$Y_3Al_5O_{12}$ is not the ideal garnet structure for doping with Nd^{3+} ions. The ionic radius of Nd^{3+} is too large to give polyhedron sides that match the sides of the Al^{3+} polyhedron. This mismatch imposes difficulties in forming a solid solution of $Nd_3Al_5O_{12}$ with $Y_3Al_5O_{12}$ that would limit the amount of Nd^{3+} that can be incorporated into the YAG lattice to only a few atomic percent. In addition, the distances between cation lattice positions for the aluminum garnets are small enough to allow for strong enough ion/ion interaction to produce concentration quenching of the Nd^{3+} fluorescence [1]†. On the other hand, neodymium may be substituted completely into gallium-based garnet systems. The largest lattice parameters in the gallium garnet group may be realized in garnets formed with lanthanum occupying the dodecahedral positions. For such garnets to be synthesized, the structure must be expanded by substitution of ions larger than gallium into the dodecahedral sites. When such substitutions were made, it was found [2] that compounds do not form with simple stoichiometry described as $\{La\}_3[Lu]_2(Ga)_3O_{12}$, but that the octahedral and tetrahedral substituents are distributed between two crystallographic sites, with the distribution corresponding to the formula $\{La_{1-x}Lu_x\}[Lu_{1-y}Ga_y]_2(Ga)_3O_{12}$.

---

yttrium aluminum garnet.

†*References are listed at the end of the text (see p 26).*

The study of mixed garnet crystals began in the late 1960's. Mixed garnets are those in which additional additives have been introduced into the $\{A\}_3[B]_2(C)_3O_{12}$ garnet crystal, causing multiple ions to occupy crystallographic sites. Numerous laboratories have studied the optical spectroscopy of mixed garnets, in particular Lu-compensated $Nd:Y_3Al_5O_{12}$. Holton et al [3] showed inhomogeneous broadening of the spectral lines of Nd^{3+}, attributed to a distribution of Nd ions among sites with different crystalline fields. The resulting broadening is attributed to Nd ions residing in Lu-rich and Y-rich sites with slightly different crystal fields. In a more comprehensive study of this mixed garnet system, Voron'ko and Sobol' [4] investigated the dependence of the width and intensity of the spectral lines with respect to varying concentrations of Y and Lu in the dodecahedral sites. A slight broadening, by 2 to 10 times, was seen in these garnets with no change of the intensities.

Doped with Nd, these mixed garnets are intermediate-gain laser materials, exhibiting gain higher than Nd:glass but lower than Nd:YAG. These materials would exhibit higher energy storage and lower amplified spontaneous emission at high pump powers [5].

2. CRYSTAL GROWTH

The lanthanum lutetium gallium garnets of the composition described above were grown by the standard Czochralski pulling technique. The raw materials were dried at 200°C, and La_2O_3 and Lu_2O_3 were fired at 1100°C for 12 hr so that they would be free of absorbed water and carbon dioxide. The oxide was then mixed in the desired ratio, pressed in an isostatic press, and loaded into a 5 × 5 cm iridium crucible. RF power at a 9.8-kHz frequency was coupled via copper coil to the crucible, heating the crucible and melting the charge. The crucible was insulated with a stabilized zirconia sleeve, and the entire assembly (coil, insulation, and crucible) was enclosed in a water-cooled bell jar equipped with nitrogen and oxygen supply lines, providing a growth atmosphere of N_2 with 1-percent volume of O_2. The pulling rates employed were 1 mm/hr. The fluid flow in the melt was aided by rotation of the crystal at the rate of 15 rpm. The crystal diameter was controlled by regulation of the weight of the growing crystal at a programmed rate. The crystal grown in the (111) direction displayed typical garnet morphology, that is, faceting and core formation due to growth with a convex interface. The crystals were 1 in. diameter and between 2 and 4 in. long. Numerous growth runs of these LLGG crystals were performed with either or both Cr^{3+} and Nd^{3+}. The samples studied were two Nd-doped boules with 3.3 and 1.0 atomic percentage added to the melt and one sample with 0.4 atomic percentage Cr^{3+}. Spectroscopic samples of high optical quality were cut and polished from these boules.

3. CRYSTAL PROPERTIES

3.1 X-Ray Diffraction

The spectroscopic characteristics of optically active ions in garnet crystals are closely related to the properties of the crystal structure. Originally determined by Menser [6] for naturally occurring minerals such as grossularite, spessartine, or pyrope, the garnet structure is cubic and belongs to space group Ia3d. All the cations are in special positions with no degree of freedom, while the oxygen atoms are in general positions. Each oxygen atom is at a shared corner of four polyhedra: one tetrahedron surrounding a "d" ion, one octahedron surrounding an "a" ion, and two dodecahedra surrounding "c" ions. The symmetry properties of these sites are summarized in table 1.

The positions of the oxygen ions in the structure are defined by three general parameters: x, y, and z. The values of these parameters change with the chemical composition of the garnets and depend mainly on the radii of the cations. When oxygen ions are shifted from their ideal positions, distortions of polyhedra result. These distortions change the length of the edges of the polyhedron, while the distances between the center and the corners of the polyhedra are given by cation/oxygen ionic radii. Thus, freedom in substitution of various cations in the garnet structure is greatly restricted by the requirement of matching the length of the shared edges among the three polyhedron types. On the other hand, expanding one polyhedron by proper selection of substituting cations may allow extending the selection of other cations for substituting into the garnet structure. This approach has been successful in doped lanthanum garnets [2].

The crystal structure analysis was performed on an automated Nicolet R3m/μ diffractometer equipped with an incident-beam graphite monochromator and Mo K_α radiation (λ = 0.7107 A*). Lattice parameters were determined for 2θ centered reflections within 3.0° < 2θ < 60.0°. Data were corrected for Lorentz-polarization effects and absorption correction. The structure of $\{La_{1-x}Lu_x\}_3[Lu_{1-y}Ga_y]_2(Ga)_3O_{12}$ was solved by direct methods by varying x and y until the R factors (or residuals) were minimized [7]. Low R factors indicate that the structure is correct and that the structure model based on atomic positions agrees well with the experimentally measured intensities. Tables 2 and 3 show the essential details of the structure; detailed structure information can be found in elsewhere.†

TABLE 1. ASPECTS OF GARNET STRUCTURE

Features	Garnet structure			
Point symmetry	222	$\bar{3}$	$\bar{4}$	1
Space group position	24c	16a	24d	96h
Typical formula	$\{Ca\}_3$	$[Al]_2$	$(Si)_3$	O_{12}
Coordination No.	8	6	4	--
Polyhedron type	Dodecahedron	Octahedron	Tetrahedron	--

*(A) + 10 = (nm)

†*T. H. Allik and C. Campana, in preparation.*

TABLE 2. SUMMARY OF SINGLE-CRYSTAL X-RAY DIFFRACTION RESULTS OF $\{La_{1-x}Lu_x\}_3[Lu_{1-x}Ga_y]_2(Ga)_3O_{12}$ for x = 0.25 AND y = 0

Ion pairs	Interatomic distances A
La-La	3.959(1)[a]
La-Lu	3.614(1)
La-Ga	3.233(1)
Lu-O	2.196(4)
La-O	2.544(5), 2.453(6)
Ga-O	1.879(6)

[a]*Parenthetical values are estimated standard deviations*
Space group: Ia3̄d (cubic)
Unit cell axis length: 12.930 (3)A
Observed data (I ≥ 3σ(I)): 236
Refinement: R = 4.07%, wR = 3.02%

TABLE 3. ATOM COORDINATES ($\times 10^4$) AND THERMAL COEFFICIENTS ($A^2 \times 10^3$) OF LLGG

Atom	x	y	z	U[a]
Lu(1)	0	0	0	21(1)
La(2)	0	2500	1250	20(1)
Lu(2)	0	2500	1250	20(1)
Ga(3)	0	2500	3750	22(1)
O	300(3)	576(3)	6569(3)	23(1)

[a]*Equivalent isotropic U defined as one-third the trace of the orthogonalized U_{ij} tensor. Also, these are estimated standard deviations.*

3.2 X-Ray Fluorescence

Elemental analysis was performed on three samples of LLGG doped with impurities: two spectroscopic samples doped with Nd^{3+} and Cr^{3+}, and another sample, a 10-cm-long by 3-cm-diameter Nd^{3+}:LLGG boule. The analysis was performed with a Kevex 770/8000 x-ray fluorescence spectrophotometer. This instrument uses the energy dispersive technique, where radiation from a primary x-ray tube is incident upon a secondary target, causing monochromatic x-ray fluorescent radiation at the K_α and K_β energy levels characteristic of the target material. This secondary radiation is then directed upon the sample to be analyzed. The subsequent x-ray fluorescence from the sample is detected and recorded on a multichannel analyzer. The chief advantage of the energy dispersive system is that secondary targets can be chosen whose secondary x-ray fluorescence will most efficiently excite the analytes in question. Such efficient monochromatic excitation results in a high signal-to-background ratio, providing the ideal conditions for accurate quantification routines.

Film standards of known concentration and mass thickness were obtained from Micromatter Co.* to obtain a known intensity/concentration ratio. This known ratio is compared with the sample fluorescence intensities and is used in conjunction with excitation efficiencies and matrix effects to calculate analyte concentrations and the elemental composition of the sample.

Micromatter Co., R. 1, Eastsound, WA 98245.

In our analysis of these samples, we selected secondary targets which would most efficiently excite the analytes of interest with minimum peak overlapping. Other parameters, such as tube voltage and current, counting time, and atmosphere, were selected to provide a statistically valid number of counts and reduce atmospheric effects. The composition of four LLGG single crystals is shown in table 4. The results in table 4 clearly indicate the added presence of lutetium in positions other than that of the octahedral site. Based on size constraints, Lu undoubtedly occupies the dodecahedral site. In addition, the Ga concentration was found to be slightly larger than three formula units, which would indicate occupancy in the octahedral site.

The segregation constant, k, for Nd^{3+}:LLGG can be determined from the data in table 4. At equilibrium, the concentration in the solid is given by [8]

$$c_s = kc_o(1 - g)^{k-1} \quad , \tag{1}$$

where c_o is the initial concentration of the dopant ion and g is the fraction of melt that has been crystallized. For Nd^{3+} in LLGG, k is 1.3.

3.3 Index of Refraction

The refractive indices of Nd:LLGG were measured using the method of minimum deviation [9], in which a polished prism of Nd^{3+}:LLGG was fabricated and mounted on a goniometer, and monochromatic light (in this case, from multiline argon ion and helium neon lasers) was passed through it. The point of least deflection is recorded as the angle of minimum deviation, and the index of refraction is calculated according to the formula

$$n = \sin[(\alpha + \eta_m)/2]/\sin(\alpha/2) \quad , \tag{2}$$

where α is the prism angle and η_m is the angle of minimum deviation. The results appear in table 5.

TABLE 4. LLGG CRYSTAL COMPOSITION IN FORMULA UNITS

Sample	Chemical analysis	Nd^{3+} concentration in LLGG composition (atomic %)	
		crystal	melt
Nd:LLGG boule (top)	$Nd_{0.04}\ La_{2.32}\ Lu_{2.57}\ Ga_{3.07}\ O_{12.00}$	1.37 ± 0.05	1.0
Nd:LLGG boule (bottom)	$Nd_{0.04}\ La_{2.26}\ Lu_{2.63}\ Ga_{3.07}\ O_{12.00}$	1.30 ± 0.05	1.0
Spectroscopic sample Nd:LLGG	$Nd_{0.13}\ La_{2.14}\ Lu_{2.53}\ Ga_{3.20}\ O_{12.00}$	4.31 ± 0.17	3.3
Spectroscopic sample Cr:LLGG	$Cr_{0.4}\ La_{2.32}\ Lu_{2.61}\ Ga_{3.07}\ O_{12.00}$	--	--

The accuracy of the refractive index calculated from the data was limited by the accuracy with which the angle of minimum deviation was measured, in this case 5 in. of arc. Thus there existed an inherent error of ±0.0025. The actual average error was ±0.0035.

These experimental data were subsequently fit to Sellmeier's dispersion equation,

$$n^2(\lambda) = 1 + S\lambda^2/(\lambda^2 - \lambda_o^2). \quad (3)$$

Appropriate values of S and λ_o, given in table 5, were calculated from this formula by averaging all the possible values extracted from the data. The index of refraction of maximum fluorescence in the $^4F_{3/2}$ to $^4I_{11/2}$ transition, 1059 nm, was found to be 1.8634.

TABLE 5. INDICES OF REFRACTION OF Nd^{3+}:LLGG

Wavelength (nm)	n experimental
632.8	1.9070
611.9	1.9174
594.1	1.9221
543.0	1.9304
514.5	1.9376
496.5	1.9537
488.0	1.9632
476.5	1.9665

Sellmeier coefficients: $n^2(\lambda) = 1 + S\lambda^2/(\lambda^2 - \lambda_o^2)$, $S = 2.3891$, $\lambda_o = 194.46$ nm.

4. NEODYMIUM SPECTRAL ANALYSIS

4.1 Nd^{3+} Absorption Spectra

The absorption spectrum of neodymium-doped LLGG was investigated in the range of 200 to 6000 nm at room temperature and 10 K. These data were recorded in the ultraviolet, visible, and near infrared on a Perkin-Elmer Lambda 9 spectrophotometer with a maximum resolution of 0.01 nm. A Perkin-Elmer 983G infrared spectrophotometer having an accuracy of 0.1 cm^{-1} was used to obtain spectra beyond 3200 nm.

A closed-cycle refrigerator, CTI-Cryogenics Model 21, was used to obtain spectra at 10 K. Sample temperatures were measured with a silicon diode calibrated to an error of less than 1 K below 50 K. Typical cooldown times were 1 hr.

Figure 1 shows the absorption spectrum at room temperature of Nd^{3+}:LLGG between 300 and 1000 nm for a 0.661-cm-thick sample with an Nd^{3+} concentration of 1.45×10^{20} ions/cm^3. This spectrum is very typical of Nd^{3+} in other crystalline hosts, showing strong transitions from the $^4I_{9/2}$ ground-state multiplet to the $^2H_{9/2}$ and $^4F_{5/2}$ (800 nm), $^4F_{7/2}$ and $^4S_{3/2}$ (750 nm), and $^4G_{5/2}$ and $^4G_{7/2}$ (590 nm) states. The experimentally determined Stark levels of the Nd^{3+} ions in the dodecahedral sites at 10 K are listed in table 6.

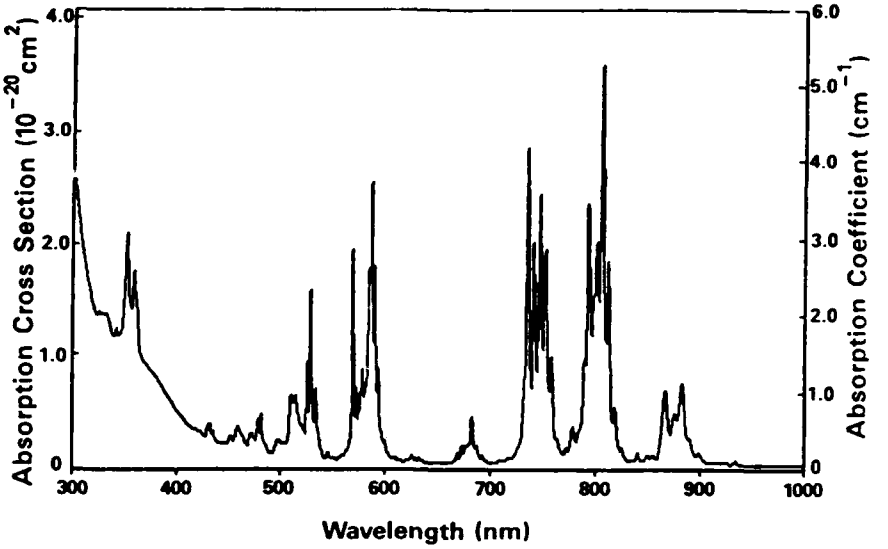

Figure 1. Room temperature absorption spectrum of Nd^{3+}:LLGG (0.5 atomic percent Nd^{3+}). Sample thickness is 6.61 mm.

The peak absorption (emission) cross section for the $^4F_{3/2}$ to $^4I_{11/2}$ (Y_3 to R_2) transition was measured. The peak absorption cross section, given in equation (4), is equal to the absorption coefficient divided by the lower-level population:

$$\sigma_p(Y_3 \rightarrow R_2) = \alpha_p(Y_3 \rightarrow R_2)/N(Y_3) \quad . \tag{4}$$

The absorption coefficient for the 10.13-cm-long Nd:LLGG boule was measured to be 6.34×10^{-4} cm^{-1}. With the Nd^{3+} concentration of the Nd:LLGG boule equal to 1.45×10^{20} Nd^{3+} ions/cm^3 (determined by x-ray fluorescence), and the partition function equal to 2.488 (data taken from table 6), the population in the Y_3 Stark level at 2097 cm^{-1} is 2.32×10^{15} Nd^{3+}/cm^3 at 298 K. Substitution of these values into equation (4) yields a cross section of 2.73×10^{-19} cm^2. This value is 2.4 and 0.9 times smaller than the values for Nd:YAG and Nd:GSGG,* respectively [10].

4.2 Branching Ratios and Radiative Lifetimes of Nd^{3+}:LLGG

The branching ratios and the radiative lifetimes of the $^4F_{3/2}$ to ^4I_J (J = 9/2, 11/2, 13/2, 15/2) were determined in two independent ways. The first method, a direct application of the Judd-Ofelt theory [11,12] has been used by many authors [13-15]. Data analysis was performed similar to that of Krupke [15] and is briefly described below.

*gadolinium scandium gallium garnet, $Gd_3Sc_2Ga_3O_{12}$.

TABLE 6. EXPERIMENTAL (E)[a] AND THEORETICAL (T)[b] CRYSTAL-FIELD SPLITTINGS OF Nd^{3+} ION MANIFOLDS IN LLGG

State[c]	Data type	Stark-level positions (cm^{-1})
$^4I_{9/2}$	E	0, 102, 187, 287, 710
313	T	-6, 103, 191, 287, 711
$^4I_{11/2}$	E	1962, 2003, 2097, 2129, 2347, 2416
2177	T	1964, 2001, 2097, 2123, 2343, 2422
$^4I_{13/2}$	E	3899, 3920, 4040, 4059, 4315, 4338, 4407
4148	T	3901, 3915, 4039, 4051, 4317, 4337, 4412
$^4I_{15/2}$	E	5783, 5818, 5959, 6009, 6450, 6481, 6526, 6603
6190	T	5784, 5824, 5963, 6006, 6454, 6473, 6525, 6588
$^4F_{3/2}$	E	11,417, 11,534
11,517	T	11,414, 11,531
$^2H_{9/2}$; $^4F_{5/2}$	E	12,402, 12,477, 12,567, 12,598, 12,625, 12,659, 12,817, 12,850
12,383; 12,652	T[d]	12,192, 12,268, 12,314, 12,452, 12,478, 12,581, 12,622, 12,656
$^4F_{7/2}$; $^4S_{3/2}$	E	13,375, 13,462, 13,582, 13,587, 13,602, 13,648
13,501; 13,592	T	13,368, 13,452, 13,564, 13,586, 13,597, 13,659
$^4F_{9/2}$	E	14,645, 14,717, 14,775, 14,852, 14,964
14,770	T	14,652, 14,723, 14,771, 14,834, 14,952
$^2H_{11/2}$	E	15,901, 15,926, 15,991, 16,093, 16,129
15,969	T[d]	15,908, 15,939, 15,961, 15,968, 16,011, 16,054
$^4G_{5/2}$; $^2G_{7/2}$	E	16,951, 17,042, 17,116, 17,324, 17,586
17,091; 17,353	T	16,963, 17,043, 17,104, 17,367, 17,434, 17,465, 17,653
$^2G_{9/2}$; $^4G_{7/2}$	E	18,825, 18,917, 18,935, 19,032, 19,361, 19,410, 19,469, 19,599, 19,650
$^2P_{1/2}$	E	23,217

[a] *Temperature (10 K)*
[b] *The crystal-field parameters given in table 9 were used in the calculation of the energy levels.*
[c] *The multiplet in Russell-Saunders notation and centroids of that multiplet are given.*
[d] *Experimental energy levels not used in the crystal-field calculations; the aqueous centroids were used instead.*

The integrated absorption coefficient, $\int k(\lambda)\, d\lambda$, emanating from the ground-state $|(SL)J\rangle$ $^4I_{9/2}$ manifold to excited $|(S'L')J1\rangle$ manifolds was measured for 11 absorption bands in figure 1. The integrated absorption coefficient in turn is related to the line strength S by equation (5) [1]:

$$\int k(\lambda)\, d\lambda = \frac{8\pi^3 N_o \bar{\lambda} e^2}{3ch(2J+1)} \left[\frac{(n^2+2)^2}{9n}\right] S \quad , \tag{5}$$

where J is the total angular momentum quantum number of the initial level, $\bar{\lambda}$ is the mean wavelength that corresponds to the J-J' transition, n is the index of refraction, and N_o is the Nd^{3+} concentration. Values for n were taken from Sellmeier's dispersion equation, equation (3), and N_o was 1.45×10^{20} ions/cm^3. The Judd-Ofelt theory predicts that the line strength S may be written in the form

$$S([SL]J;[S'L']J') = \sum_{t=2,4,6} \Omega_t |\langle 4f^n[SL]J||U^{(t)}||4f^n[S'L']J'\rangle|^2 , \qquad (6)$$

where $\langle 4f^n[SL]J||U^{(t)}||4f^n[S'L']J'\rangle$ is a reduced-matrix element of the irreducible tensor operator of rank t, and Ω_t are the Judd-Ofelt parameters. The numerical values of the squares of the reduced-matrix elements for Nd^{3+} (aqua) ions for transitions from the ground state were taken from Carnall, Fields, and Rajnak [16]. When the absorption band was a superposition of lines assigned to several intermultiplet transitions, the matrix element was taken to be the sum of the corresponding squared matrix elements [1]. A least-squares fitting of S_{calc} to S_{meas} yields values for $\Omega_{2,4,6}$. Table 7 shows the measured and calculated line strengths for 11 absorption bands. The Judd-Ofelt parameters and the branching ratios are given in table 8.

TABLE 7. MEASURED AND CALCULATED LINE STRENGTHS OF Nd^{3+} IN LLGG

Russel-Saunders state [S'L']J'	Wavelength (nm)	Index of refraction n	Line strengths (10^{-20} cm^2)	
			S_{meas}	S_{calc}
$^4F_{3/2}$	882	1.8738	0.424	0.749
$^4F_{5/2} + {}^2H_{9/2}$	807	1.8805	2.137	1.984
$^4F_{7/2} + {}^4S_{3/2}$	748	1.8874	1.741	1.842
$^4F_{9/2}$	683	1.8973	0.144	0.133
$^2H_{11/2}$	625	1.9092	0.014	0.034
$^4G_{5/2} + {}^2G_{7/2}$	587	1.9193	1.594	1.594
$^2K_{13/2} + {}^4G_{7/2} + {}^4G_{9/2}$	526	1.9410	0.886	0.898
$^2K_{15/2} + {}^2G_{9/2} + ({}^2D,{}^2P)_{3/2}$	479	1.9648	0.130	0.176
$^4G_{11/2}$	459	1.9778	0.084	0.016
$^2P_{1/2} + {}^2D_{5/2}$	433	1.9982	0.041	0.103
$^2P_{3/2} + {}^2D_{3/2}$	356	2.0988	0.980	0.789

The second method of determining the branching ratios and radiative lifetimes uses the point charge model. In these calculations, the experimentally determined Stark-level positions of Nd^{3+} given in table 6 were used along with the free-ion Russell-Saunders [SL]J states with the free-ion Hamiltonian containing the Coulomb, spin-orbit, L^2, $G(G_2)$, and $G(R_7)$ interactions [17]. The free-ion parameters chosen, from Carnall, Fields, and Rajnak [16], are $E^{(1)}$= 4739.3, $E^{(2)}$= 23.999, $E^{(3)}$= 485.96, ζ = 884.58, α = 0.5611, β = -117.15, γ = 1321.3 (all in cm^{-1}). In the crystal-field analysis we assume a crystal field of D_2 symmetry of the form

TABLE 8. EXPERIMENTAL AND THEORETICAL JUDD-OFELT PARAMETERS AND PREDICTED BRANCHING RATIOS IN Nd^{3+}:LLGG

Quantity	Experimental Ω_k	Theoretical Ω_k
Judd-Ofelt parameters ($\times 10^{-20}/cm^2$)		
Ω_2	0.84	0.317
Ω_4	2.64	1.206
Ω_6	2.61	5.186
Radiative lifetime (μs)		
$^4F_{3/2}$	362,[a] 295[b]	286
Branching ratios (%)		
$\beta(^4F_{3/2}-^4I_{9/2})$	43.6	26.0
$\beta(^4F_{3/2}-^4I_{11/2})$	47.2	59.5
$\beta(^4F_{3/2}-^4I_{13/2})$	8.8	13.8
$\beta(^4F_{3/2}-^4I_{15/2})$	0.4	0.7

[a] *From Judd-Ofelt calculations.*
[b] *From fluorescence lifetime experiments.*

$$H_{CEF} = \sum_{ikq} B^*_{kq} C_{kq}(\hat{r}_i) \quad , \tag{7}$$

where the B_{kq} are the crystal-field parameters, and the $C_{kq}(\hat{r})$ are spherical tensors related to the spherical harmonics by

$$C_{kq}(\hat{r}_i) = \sqrt{4\pi/(2k+1)}\, Y_{kq}(\theta_i, \phi_i) \quad . \tag{8}$$

The sum on i in equation (7) runs over the three electrons in the $4f^3$ configuration of Nd^{3+}, and the sum on k (k even) covers the range 2 through 6 with q even and in the range $-k \leq q \leq k$. Since we assume that the Nd^{3+} ions occupy the dodecahedral site with D_2 symmetry, the crystal-field parameters can be chosen real; thus there is a total of nine even-k B_{kq}. The procedure we use in the analysis of the experimental data is to obtain the free-ion wave functions using the free-ion parameters. We then use these free-ion wave functions to evaluate the energy levels in a crystal using the Hamiltonian given in equation (7). The crystal-field parameters B_{kq} are then determined by minimizing the squared difference of the calculated energies from the experimental energies. The centroids of each [SL]J multiplet are allowed to vary freely during this fitting and are considered experimental data in the final analysis.

To obtain starting values of B_{kq} for our fitting of the experimental energy levels, we use point-charge lattice sums A_{kq}. The A_{kq} are related to the B_{kq} by [18]

$$B_{kq} = \rho_k A_{kq} \quad , \tag{9}$$

where

$$\rho_k = \tau^{-k} \langle r^k \rangle_{HF} (1 - \sigma_k) \quad , \tag{10}$$

where τ is an ion-dependent radial expansion parameter [18], $\langle r^k \rangle_{HF}$ are Hartree-Fock expectation values [19], and σ_k are shielding factors [20]. Values of ρ_k for Ce^{3+} through Yb^{3+} are given by Morrison and Leavitt [21]. The values of A_{kq} were calculated by a point-charge lattice sum using the x-ray data of table 3. In performing the lattice sum, we assume that the material is $La_3Lu_2Ga_3O_{12}$, and that for the starting parameters the charges on the individual ions are the valence charges $q_{La} = 3$, $q_{Lu} = 3$, $q_{Ga} = 3$, and $q_O = -2$ (in units of the electron charge). Later we calculated A_{kq} using an effective charge on the oxygen site q_O such that $q_{Ga} = -5 - 4q_O$ and varying q_O to obtain the best fit of calculated B_{kq} to experimental B_{kq}. The resulting A_{kq} for even k were obtained from the lattice sums; the B_{kq} obtained by using equation (9) are given in column 3 of table 9. These values of B_{kq} were used in the least-squares fitting as starting parameters.

TABLE 9. EXPERIMENTAL AND CALCULATED CRYSTAL-FIELD PARAMETERS, B_{kq} (cm^{-1})

kq	Best-fit experimental B_{kq} [a]	Point-charge B_{kq} [b]
20	879	843
22	206	338
40	-80.4	68.6
42	-1650	-2370
44	-782	-1087
60	-1345	-1485
62	-608	-732
64	629	736
66	-613	-614

[a] Best-fit experimental B_{kq} for all data, rms = 5.658 cm^{-1}.

[b] Point-charge B_{kq} using $q_O = -1.64$, rms = 50.38 cm^{-1}.

Note: Odd-k A_{kq}(cm^{-1}/A^k) for $q_O = -1.64$, $A_{32} = 1520$, $A_{52} = -1500$, $A_4 = 867$, $A_{72} = 54.2$, $A_{74} = 88.0$, and $A_{76} = -129$.

The crystal-field parameters that gave the best fit to the experimental data are given in table 9, as well as the point-charge B_{kq} computed using $q_O = -1.64$ (the value of the oxygen charge that gave the best agreement to the experimental B_{kq}). In this fitting a number of experimental levels were discarded because attempts to fit these levels were unsuccessful. The odd-k A_{kq} (cm^{-1}/A^k) using $q_O = -1.64$ were calculated and are $A_{32} = 1520$, $A_{52} = -1500$, $A_{54} = 867$, $A_{72} = 54.2$, $A_{74} = 88.0$, and $A_{76} = -129$. (All odd-k A_{kq} are imaginary.)

The B_{kq} of table 9, along with the odd-k A_{kq} values, were used to calculate the intensity of electric- and magnetic-dipole transitions for the rare-earth series. A detailed discussion of this calculation is given by Leavitt and Morrison [22]. The resulting Judd-Ofelt intensity parameters are given in table 8 for Nd^{3+}, along with the radiative lifetime of the $^4F_{3/2}$ state and the branching ratios to the ^4I_J manifolds. The Judd-Ofelt parameters for the other rare earths are given in table 10.

4.3 Nd^{3+}:LLGG Fluorescence and Lifetime Measurements

The fluorescence spectrum of Nd^{3+}:LLGG was recorded with a Spex F222 spectrometer. Figures 2 and 3 show the fluorescence spectrum in the region of the $^4F_{3/2}$ to $^4I_{11/2}$ and $^4F_{3/2}$ to $^4I_{9/2}$ transitions. The fluorescence lifetime and time-resolved, site-selection spectroscopy measurements were made with a nitrogen laser-pumped tunable dye laser with rhodamine 6G for the excitation source. This provided pulses of about 10 ns in duration and less than 0.04 nm halfwidth. The sample was mounted in a cryogenic refrigerator with a temperature variable between 10 and 300 K. The fluorescence was analyzed by a 1-m monochromator, detected by a cooled RCA C31034 photomultiplier tube, processed by an EGG-PAR boxcar integrator triggered by the laser, and displayed on an x-y recorder.

The fluorescence lifetime of Nd^{3+} in LLGG after lower power dye laser excitation varies from about 290 μs at 11 K to about 205 μs at room temperature, as shown in figure 4. The solid line in the figure represents the best fit to the data using an expression of the form

$$\tau_f^{-1} = \tau_r^{-1} + C\{\exp[\Delta E/(k_B T)] - 1\}^{-1} \quad , \tag{11}$$

where τ_f and τ_r are the fluorescence and radiative lifetimes, respectively. The last term describes the quenching of the lifetime due to radiationless processes involving the absorption of phonons of energy ΔE. C is a constant containing the matrix element for these transitions. The values obtained from fitting equation (11) to the experimental data are listed in table 11. Several types of processes can lead to this type of lifetime quenching and will be discussed in section 5.2.

TABLE 10. CALCULATED JUDD-OFELT INTENSITY PARAMETERS Ω_k OF RARE-EARTH IONS IN La SITE OF $La_3Lu_2Ga_3O_{12}$

Ion	J. O. intensity parameters (10^{-20} cm^2)			Ion	J. O. intensity parameters (10^{-20} cm^{-2})		
	Ω_2	Ω_4	Ω_6		Ω_2	Ω_4	Ω_6
Ce	0.5872	3.734	22.17	Tb	0.1729	0.8314	3.913
Pr	0.3286	1.884	9.449	Dy	0.1271	0.5830	2.428
Nd	0.3167	1.206	5.186	Ho	0.1038	0.4601	1.772
Pm	0.1833	0.9318	3.986	Er	0.0095	0.4352	1.671
Sm	0.1599	0.7902	3.300	TM	0.0968	0.4190	1.615
Eu	0.1265	0.6060	2.333	Yb	0.0817	0.3417	1.230
Gd	0.0990	0.4588	1.610				

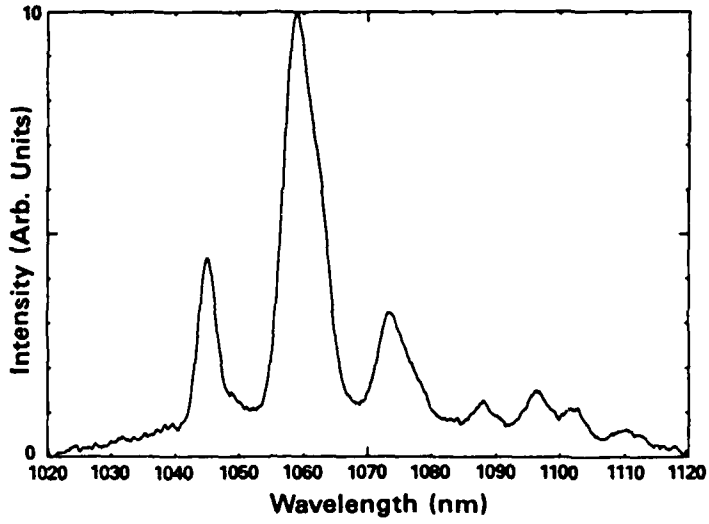

Figure 2. Fluorescence of Nd^{3+}:LLGG at room temperature in region of $^4F_{3/2}$-$^4I_{11/2}$.

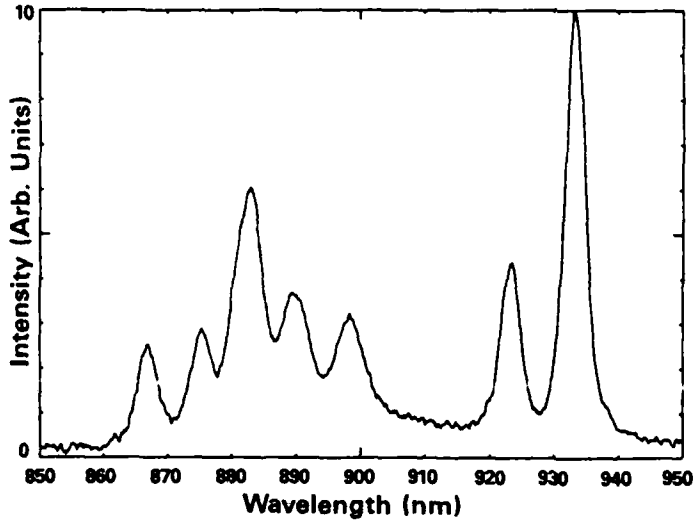

Figure 3. Fluorescence of Nd^{3+}:LLGG at room temperature in region of $^4F_{3/2}$-$^4I_{9/2}$.

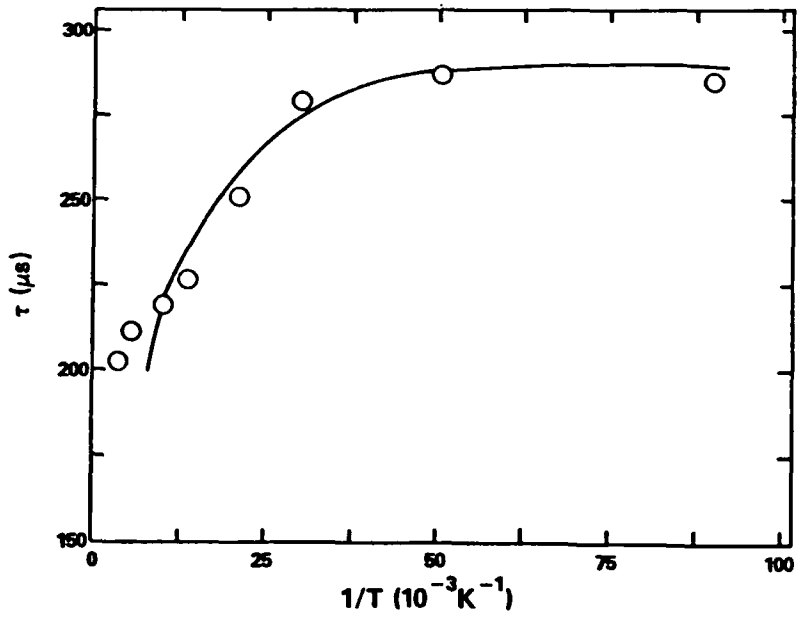

Figure 4. Temperature dependence of fluorescence lifetime of $^4F_{3/2}$ metastable state of Nd^{3+}:LLGG. (See text for explanation of theoretical line.)

TABLE 11. SUMMARY OF PARAMETERS

Parameter	Value
τ_f $^4F_{3/2}$(10 K)	290 μs
τ_f $^4F_{3/2}$(300 K)	205 μs
τ_r $^4F_{3/2}$	295 μs
τ_f $^2P_{3/2}$(300 K)	0.32 μs
τ_{rt} $^2P_{3/2}$(300 K)	317 ns
τ_f $^2(F2)_{5/2}$(300 K)	2.52 μs
τ_{rt} $^2(F2)_{5/2}$(300 K)	200 ns
c	1538 μs
ΔE	30 cm^{-1}
a (100 K)	392 μs
ΔE_s	29 cm^{-1}

5. INVESTIGATIONS FOR LASER APPLICATIONS

5.1 Laser Gain Measurements

The laser-pumped, single-pass gain measurements using the frequency-doubled output of a mode-locked Nd:YAG laser as the pump source were performed at Oklahoma State University. This laser provided a 25-ps excitation pulse with a few millijoules of energy at 532 nm. The probe beam was the collimated output of a xenon lamp passed through a 0.5-m monochromator. The change in the probe beam transmission through the sample under pumped conditions was monitored with a 0.25-m monochromator and photomultiplier tube with the output photographed on a storage scope. Multiphoton excitation studies were made with the same laser for excitation, and the fluorescence emission was monitored with a 0.25-m monochromator with an EGG-PAR silicon array detector and optical multichannel analyzer (OMA) combination. Fluorescence lifetimes under these excitation conditions were again measured with the boxcar integrator.

The attempt to observe single-pass gain was made with the probe beam tuned to the emission peak at 1059 nm while the pump beam at 532 nm was in resonance with one of the strong absorption transitions. Although these experimental conditions resulted in easily observable gain for several different types of Nd-doped crystal and glass materials, no gain was observed for the LLGG sample at room temperature. Since the optical quality (and thus the scattering losses per pass) was approximately the same for each of the samples investigated, the lack of optical gain indicates the presence of some type of loss process occurring for Nd^{3+} in the LLGG host.

Direct lasing of two Nd:LLGG samples was attempted at the Center for Night Vision and Electro-Optics. Two experiments were performed with different wavelengths of excitation and different pumping geometries. A laser diode array capable of producing 80 mJ per pulse at 20 Hz was used as a pump at 808 nm in a side-pump geometry. Typical outputs for Nd:YAG with the use of this scheme are 25 mJ.* When an Nd:LLGG sample was inserted in the resonator, no lasing was detected at 1059 nm. End-pumping of the same crystal was also attempted with a Coherent 699-29 ring dye laser producing 1.3 W with rhodamine 6G. Lasing was not detected at 1059 nm. A focused dye laser beam at 595 nm produced an intense purple fluorescence at the focal point. This is consistent with the experimental results shown in section 5.2.

5.2 Multiphoton Excitation Measurements

For low excitation powers, the fluorescence emission originates from the $^4F_{3/2}$ metastable state at wavelengths longer than 850 nm. After high-power picosecond pulse pumping, fluorescence emission extends throughout the visible region of the spectrum to about 800 nm, as shown in figure 5. This

*D. Caffey, private communication.

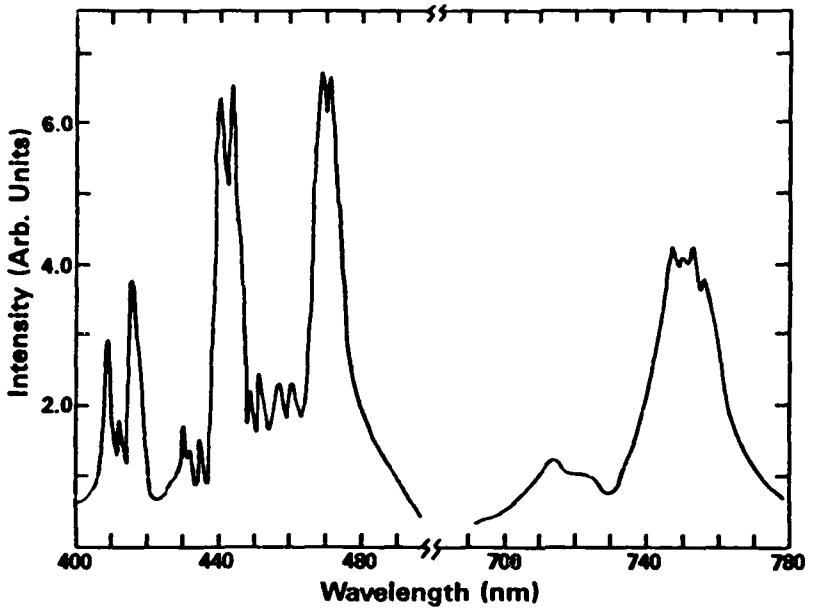

Figure 5. Fluorescence of Nd^{3+}:LLGG at room temperature after pumping at 532 nm with a 25-ps laser pulse.

demonstrates the presence of multiphoton excitation processes and subsequent emission from higher energy metastable states. The spectral dynamics occurring under these pumping conditions have been studied for Nd^{3+} in YAG, $Y_3Ga_5O_{12}$ (yttrium gallium garnet--YGG) and lithium silicate glass [23,24]. The transitions have been shown to originate on the $^2P_{3/2}$ and $^2F_{5/2}$ metastable states with lifetimes of about 0.3 and 3.0 μs, respectively. The fluorescence lines shown in figure 5 can be divided into one set having a lifetime of 0.3 μs and another set having a lifetime of 2.5 μs. In comparison to the previous results, we assign these transitions to lines originating on the $^2P_{2/3}$ and $^2(F2)_{5/2}$ states, respectively.

One important difference between the results obtained on Nd^{3+}:LLGG and those obtained on other hosts is that strong emission from the $^4F_{3/2}$ level was observed for the other samples under these pumping conditions [23,24] but not for LLGG. This implies that multiphoton excitation transitions lead to relaxation channels that bypass the $^4F_{3/2}$ metastable state and thus act as a loss mechanism for pumping the $^4F_{3/2}$ to $^4I_{11/2}$ laser transition. The multiphoton processes in the other hosts have been shown to be sequential two-photon excitation processes (STEP's) involving a real intermediate state [24], and we assume that the same mechanism is active in LLGG. The effects of the STEP mechanism appear to be stronger in the LLGG sample than in the other

hosts. One important spectral difference that may account for this is that the 532-nm pump wavelength is almost exactly in resonance with an absorption transition in LLGG, whereas for the other hosts investigated this wavelength is on the wing of the absorption band.

5.3 Energy Transfer Measurements

Dye laser, time-resolved spectroscopy techniques were used to investigate the characteristics of energy transfer between Nd^{3+} ions in nonequivalent crystal-field sites in the region from 560 to 600 nm. The fluorescence in the 880-nm spectral region was monitored in this investigation and is shown in figure 6 for two temperatures. At 11 K these transitions are associated with emission from the $^4F_{3/2}$ metastable state to the various Stark components of the $^4I_{9/2}$ ground-state manifold. At room temperature, emission from higher excited states is present, and the transitions broaden because of both electron/phonon interactions and energy transfer to ions in spectrally inequivalent sites.

Microscopic strains produce slightly different crystal fields at the site of each Nd^{3+} ion in the lattice, resulting in inhomogeneous broadening of the spectral lines. In addition, Nd^{3+} ions occupying sites having significantly different crystal-field environments produce transitions that are easily resolvable in the optical spectra. Ions in a specific type of site can

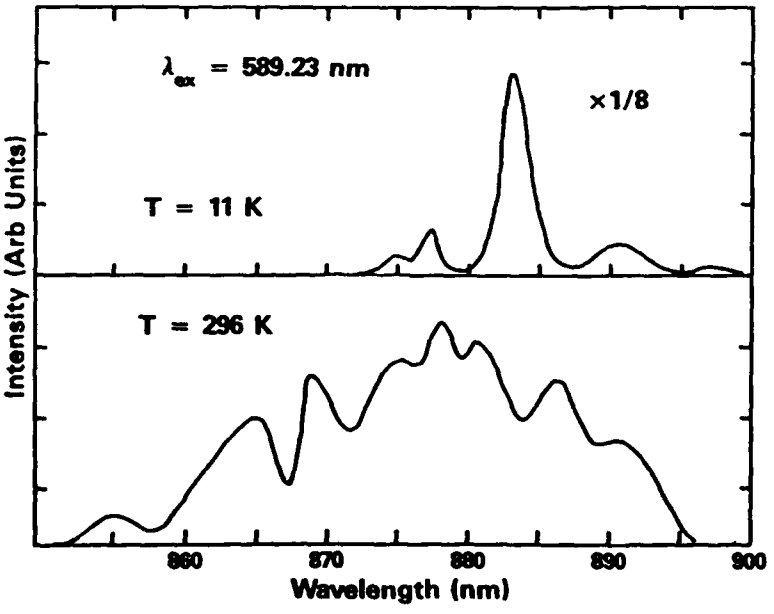

Figure 6. Fluorescence of Nd^{3+}:LLGG at two temperatures in region of $^4F_{3/2}$-$^4I_{9/2}$ transition after pumping near 589 nm with a 10-ns laser pulse.

be selectively excited by tuning the dye laser into resonance with one of the absorption transitions associated with these ions. The results of doing this are shown in figure 7. As the excitation wavelength is tuned over 0.41 nm, the maximum emission of this transition shifts from peak a to peak b, indicating a change in the type of ion being excited. Note that the energy separation of the transitions originating from the ions in these two types of sites is $\Delta E_s = 29\ cm^{-1}$.

In order to study the energy transfer between Nd^{3+} ions in these two major types of sites, the time evolution of the relative fluorescence intensities of peaks a and b was monitored as a function of time after the excitation pulse for both excitation wavelengths. These time-resolved measurements were carried out at several temperatures between 11 and 100 K, above which the thermal broadening of the lines prevented the spectral resolution necessary for accurate measurements. In this temperature range, no variation was observed in the ratios of the intensities of peaks a and b as a function of time. This indicates that energy transfer between Nd^{3+} ions in these two different types of sites is a very weak process. However, the similarity of the activation energy for thermal quenching of the fluorescence lifetime and the energy difference between peaks a and b may indicate that at higher temperatures energy transfer between ions in these two major types of sites does occur and results in the quenching of the decay time.

Even though energy transfer between ions in the two major types of sites is negligible at low temperatures, time-resolved spectroscopy measurements do reveal spectral energy transfer across an inhomogeneously broadened line. An example of this is shown in figure 8, where the shape of fluorescence transition a is shown for two times after the laser pulse at 100 K. A distinct high-energy shoulder appears on this line at short times and disappears at long times. This can be attributed to the presence of energy transfer between Nd^{3+} ions in type a sites with differences in transition energies due to local perturbations of their surrounding crystal fields. This type of energy transfer can be treated quantitatively in the formalism developed for analyzing spectral energy transfer in doped glasses [25]. In this model, the time evolution of the fluorescence intensity at frequency ω is expressed as

$$I(\omega,t) = a(t)I(\omega,0) + [1 - a(t)]I(\omega,\infty) \quad , \tag{12}$$

where a(t) is the function describing the energy transfer. This can be integrated to give

$$a(t) = \int_{\omega_1}^{\omega_2} [I(\omega,t) - I(\omega,\infty)]\, d\omega + \int_{\omega_1}^{\omega_2} I(\omega,0) - I(\omega,\infty)]\, d\omega \quad . \qquad (13)$$

The results of this analysis at 100 K are plotted in figure 9. The energy transfer function decreases exponentially with time, having a characteristic time constant of α = 392 μs. The energy transfer parameters are summarized in table 11.

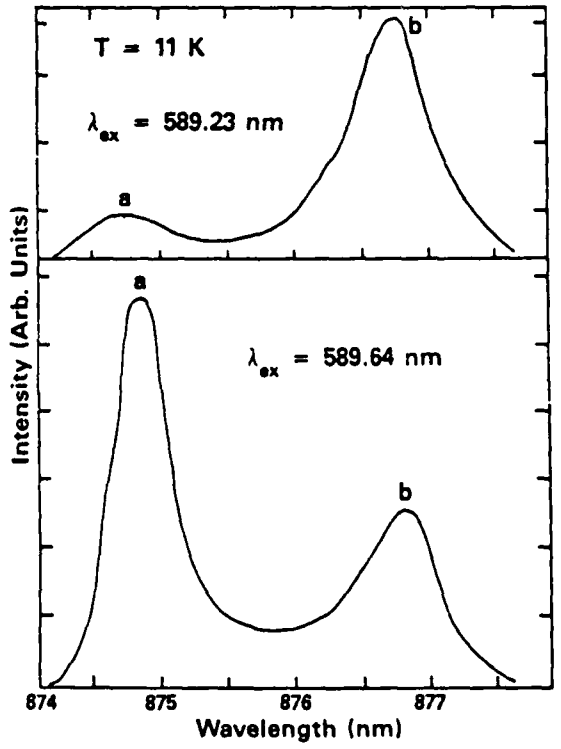

Figure 7. Fluorescence of Nd^{3+}:LLGG at 11 K in region of one of $^4F_{3/2}$-$^4I_{9/2}$ transitions for two different excitation wavelengths.

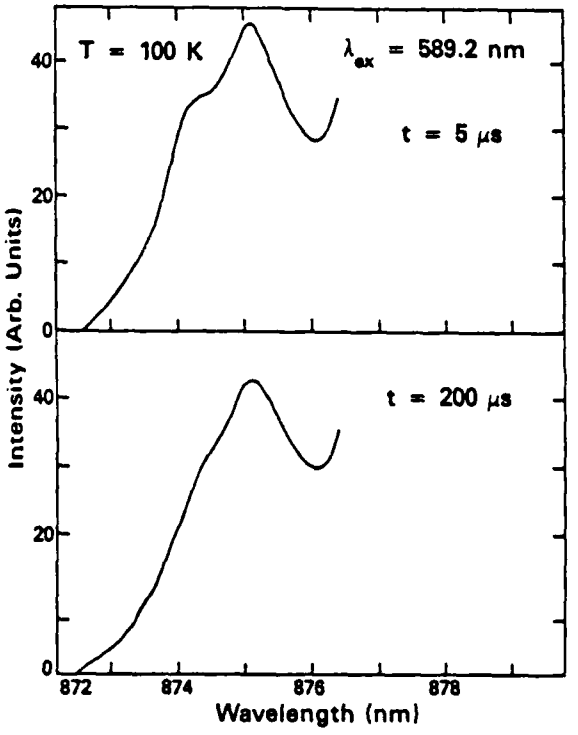

Figure 8. Fluorescence of Nd^{3+}:LLGG at 100 K in 875-nm spectral region at two different times after excitation pulse.

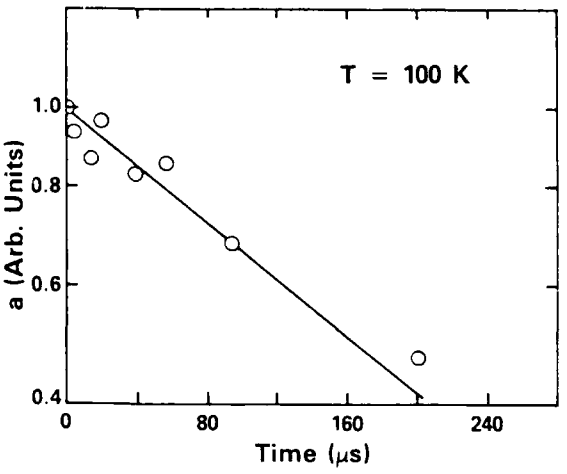

Figure 9. Time dependence of energy transfer function a(t) at 100 K obtained from equation (13) by monitoring time evolution of shape of fluorescence band at 875 nm.

6. SUMMARY AND CONCLUSIONS

The lifetime results summarized in table 11 indicate that Nd^{3+} ions in LLGG have a quantum efficiency near 98 percent, which is significantly higher than that for Nd:YAG crystals with this doping concentration [1]. In addition, the rate of energy transfer between ions in the two major types of nonequivalent crystal-field sites is much smaller than in the YAG host [26]. Since the quantum efficiency of $^4F_{3/2}$ fluorescence in Nd^{3+}-doped materials is generally attributed to cross-relaxation processes between neighboring Nd^{3+} ions which can be enhanced by energy migration among the Nd^{3+} ions, these results are indicative of weak ion/ion interaction processes in the LLGG host. This observation is consistent with the increased ion/ion separation in the LLGG crystal.

The origin of the two major types of nonequivalent crystal-field sites in LLGG has not been identified. However, in comparison with the results of previous site-selection spectroscopy investigations of mixed garnet crystals [3,26], it is reasonable to assume that the different sites are associated with different lutetium environments around the Nd^{3+} ions. In the YAG host, the energy transfer between ions in the different types of sites has been attributed to a two-phonon assisted process with a real intermediate state [26]. This leads to an activation energy associated with the energy level splitting of the lowest two ground-state Stark components, which is

significantly greater than the measured activation energy in the Nd^{3+}:LLGG crystal. This implies the presence of different types of energy transfer mechanisms in the two types of hosts.

The point-charge calculation of the odd-fold crystal fields (odd-k A_{kq}) was used to calculate the Judd-Ofelt intensity parameters, Ω_k, for all the rare-earth experimental values. For Nd^{3+}:LLGG the radiative lifetime of the $^4F_{3/2}$ level was calculated and compares favorably with experiment. The branching ratio from a line-to-line intensity calculation for the $^4F_{3/2}$ to ^4I_J manifold was determined. The agreement of the crystal-field calculations with the experimental data was excellent for the ^4I_J and ^4F_J multiplets as well as the $^4S_{3/2}$ and $^4G_{5/2}$ energy levels.

The ability to incorporate high concentrations of Nd^{3+} in the lattice without degrading the optical quality and maintaining a high level of quantum efficiency would make LLGG an attractive host for an Nd^{3+} laser material. However, our inability to observe optical gain under pumping conditions producing gain in other Nd-doped materials and the presence of strong multiphoton transitions eliminate Nd^{3+}:LLGG as a replacement for Nd^{3+}:YAG or Nd^{3+}:Cr^{3+}:GSGG as a 1-μm laser.

ACKNOWLEDGMENTS

The Oklahoma State University part of this research was sponsored by the U.S. Army Research Office. The Science Applications International Corporation (SAIC) work was sponsored by the Center for Night Vision and Electro-Optics. One of the authors (D. K. Sardar) gratefully acknowledges financial support from the University of Texas at San Antonio for this work.

LITERATURE CITED

(1) A. A. Kaminskii, Laser Crystals, Springer-Verlag, Berlin (1981).

(2) M. Kokta and M. Grasso, J. Solid State Chem. 8 (1973), 357.

(3) L. A. Riseberg and W. C. Holton, J. Appl. Phys. 43 (1972), 1876; L. A. Riseberg, R. M. Brown, and W. C. Holton, Appl. Phys. Lett. 23 (1973), 127; L. A. Riseberg and W. C. Holton, Opt. Commun. 9 (1973), 298.

(4) Yu. K. Voron'ko and A. A. Sobol', Trudy Ordena Lenima Fizicheskogo Instituta Im. P. N. Lebedeva, 98:39 (1982).

(5) W. Koechner, Solid State Laser Engineering, Vol. 1, Springer-Verlag, New York (1976), p. 35.

(6) G. Menser, Z. Kristallogr. 63 (1926), 157.

(7) J. D. Dunitz, X-Ray Analysis and the Structure of Organic Molecules, Cornell University Press, NY (1979), pp 183-222.

(8) B. R. Pamplin, Crystal Growth, Vol. 16, Pergamon Press, Oxford (1980) p 289.

(9) W. L. Bond, J. Appl. Phys. 36 (1965), 1674.

(10) W. F. Krupke, M. D. Shinn, J. E. Marion, J. A. Caird, and S. E. Stokowski, J. Opt. Soc. Am. B 3 (1986), 102.

(11) B. R. Judd, Phys. Rev. 127 (1962), 750.

(12) G. S. Ofelt, J. Chem. Phys. 37 (1962), 511.

(13) M. J. Weber, T. E. Varitmos, and B. H. Matsinger, Phys. Rev. B8 (1973), 47.

(14) W. F. Krupke, IEEE J. Quantum Electron. QE-10 (1974), 450.

(15) W. F. Krupke, IEEE J. Quantum Electron. QE-7 (1971), 153.

(16) W. T. Carnall, P. R. Fields, and K. Rajnak, J. Chem. Phys. 49 (1968) (five consecutive papers), 4412-55.

(17) B. G. Wybourne, Spectroscopic Properties of Rare Earths, Wiley, NY (1965).

(18) C. A. Morrison, N. Karayianis, and D. E. Wortman, Rare Earth Ion-Host Lattice Interactions 4. Predicting Spectra and Intensities of Lanthanides in Crystals, Harry Diamond Laboratories, HDL-TR-1816 (June 1977).

LITERATURE CITED (cont'd)

(19) A. J. Freeman and R. E. Watson, Phys. Rev. 127 (1962), 2058.

(20) P. Erdos and J. H. Kang, Phys. Rev. B6 (1972), 3393.

(21) C. A. Morrison and R. P. Leavitt, J. Chem. Phys. 71 (1979), 2366.

(22) R. P. Leavitt and C. A. Morrison, J. Chem. Phys. 73 (1980), 749.

(23) G. E. Venikouas, G. J. Quarles, J. P. King, and R. C. Powell, Phys. Rev. B30 (1984), 2401.

(24) G. J. Quarles, G. E. Venikouas, and R. C. Powell, Phys. Rev. B31 (1985), 6935.

(25) S. A. Brawer and M. J. Weber, Appl. Phys. Lett. 35 (1979), 31.

(26) L. D. Merkle and R. C. Powell, Phys. Rev. B20 (1979), 75; M. Zokai, R. C. Powell, G. F. Imbusch, and B. DiBartolo, J. Appl. Phys. 50 (1979), 5930.

DISTRIBUTION

ADMINISTRATOR
DEFENSE TECHNICAL INFORMATION CENTER
ATTN DTIC-DDA (12 COPIES)
CAMERON STATION, BUILDING 5
ALEXANDRIA, VA 22314

DIRECTOR
NIGHT VISION & ELECTRO-OPTICS LABORATORY
ATTN TECHNICAL LIBRARY
ATTN R. BUSER
ATTN A. PINTO (10 COPIES)
ATTN J. HABERSAT
ATTN W. HOVIS (10 COPIES)
FT BELVOIR, VA 22060

DIRECTOR
DEFENSE ADVANCED RESEARCH
PROJECTS AGENCY
ATTN J. FRIEBELE
1400 WILSON BLVD
ARLINGTON, VA 22209

DIRECTOR
DEFENSE NUCLEAR AGENCY
ATTN TECH LIBRARY
WASHINGTON, DC 20305

UNDER SECRETARY OF DEFENSE RES
& ENGINEERING
ATTN TECHNICAL LIBRARY, 3C128
WASHINGTON, DC 20301

OFFICE OF THE DEPUTY CHIEF OF STAFF,
FOR RESEARCH, DEVELOPMENT,
& ACQUISITION
DEPARTMENT OF THE ARMY
ATTN DAMA-ARZ-A, CHIEF SCIENTIST,
L. CAMERON
ATTN DAMA-ARZ-B, I. R. HERSHNER
WASHINGTON, DC 20310

COMMANDER
US ARMY ARMAMENT MUNITIONS &
CHEMICAL COMMAND (AMCCOM)
US ARMY ARMAMENT RESEARCH &
DEVELOPMENT CENTER
ATTN DRDAR-TSS, STINFO DIV
DOVER, NJ 07801

COMMANDER
ATMOSPHERIC SCIENCES LABORATORY
ATTN TECHNICAL LIBRARY
WHITE SANDS MISSILE RANGE, NM 88002

DIRECTOR
US ARMY BALLISTIC RESEARCH LABORATORY
ATTN DRDAR-TSB-S (STINFO)
ABERDEEN PROVING GROUND, MD 21005

DIRECTOR
US ARMY ELECTRONICS WARFARE LABORATORY
ATTN J. CHARLTON
ATTN DELET-DD
FT MONMOUTH, NJ 07703

COMMANDING OFFICER
USA FOREIGN SCIENCE & TECHNOLOGY CENTER
FEDERAL OFFICE BUILDING
ATTN DRXST-BS, BASIC SCIENCE DIV
CHARLOTTESVILLE, VA 22901

COMMANDER
US ARMY MATERIALS & MECHANICS
RESEARCH CENTER
ATTN DRXMR-TL, TECH LIBRARY
WATERTOWN, MA 02172

US ARMY MATERIEL COMMAND
5001 EISENHOWER AVE
ALEXANDRIA, VA 22333-0001

US ARMY MATERIEL SYSTEMS ANALYSIS
ACTIVITY
ATTN DRXSY-MP (LIBRARY)
ABERDEEN PROVING GROUND, MD 21005

COMMANDER
US ARMY MISSILE & MUNITIONS
CENTER & SCHOOL
ATTN ATSK-CTD-F
ATTN DRDMI-TB, REDSTONE SCI INFO CENTER
REDSTONE ARSENAL, AL 35809

COMMANDER
US ARMY RESEARCH OFFICE (DURHAM)
PO BOX 12211
ATTN ROBERT J. LONTZ
ATTN M. STROSIO
ATTN M. CIFTAN
ATTN B. D. GUENTHER
ATTN CHARLES BOGOSIAN
RESEARCH TRIANGLE PARK, NC 27709

COMMANDER
US ARMY RSCH & STD GRP (EUROPE)
FPO NEW YORK 09510

COMMANDER
US ARMY TEST & EVALUATION COMMAND
ATTN D. H. SLINEY
ATTN TECH LIBRARY
ABERDEEN PROVING GROUND, MD 21005

COMMANDER
US ARMY TROOP SUPPORT COMMAND
ATTN DRXRES-RTL, TECH LIBRARY
NATICK, MA 01762

DISTRIBUTION

OFFICE OF NAVAL RESEARCH
ATTN J. MURDAY
ARLINGTON, VA 22217

DIRECTOR
NAVAL RESEARCH LABORATORY
ATTN CODE 2620, TECH LIBRARY BR
ATTN CODE 6551, F. BARTOLI
ATTN CODE 6551, L. ESTEROWITZ
ATTN CODE 6551, R. E. ALLEN
ATTN CODE 6551, G. KINTZ
WASHINGTON, DC 20375

HQ, USAF/SAMI
WASHINGTON, DC 20330

DEPARTMENT OF COMMERCE
NATIONAL BUREAU OF STANDARDS
ATTN LIBRARY
WASHINGTON, DC 20234

NASA LANGLEY
ATTN N. BARNES
ATTN P. L. CROSS
HAMPTON, VA 23665

DIRECTOR
ADVISORY GROUP ON ELECTRON DEVICES
ATTN SECTRY, WORKING GROUP D
201 VARICK STREET
NEW YORK, NY 10013

AEROSPACE CORPORATION
PO BOX 92957
ATTN M. BIRNBAUM
ATTN N. C. CHANG
LOS ANGELES, CA 90009

COLORADO STATE UNIVERSITY
PHYSICS DEPARTMENT
ATTN S. KERN
FORT COLLINS, CO 80523

ALLIED
ADVANCED APPLICATION DEPT
ATTN A. BUDGOR
31717 LA TIEMDA DRIVE
WESTLAKE VILLAGE, CA 91362

AMES LABORATORY DOE
IOWA STATE UNIVERSITY
ATTN K. A. GSCHNEIDNER, JR. (2 COPIES)
AMES, IA 50011

ARGONNE NATIONAL LABORATORY
ATTN W. T. CARNALL
ATTN H. M. CROSSWHITE
9700 SOUTH CASS AVENUE
ARGONNE, IL 60439

ARIZONA STATE UNIVERSITY
DEPT OF CHEMISTRY
ATTN L. EYRING
TEMPE, AZ 85281

BRIMROSE CORP OF AMERICA
ATTN R. G. ROSEMEIER
7527 BELAIR ROAD
BALTIMORE, MD 21236

CARNEGIE MELLON UNIVERSITY
SCHENLEY PARK
ATTN PHYSICS & EE, J. O. ARTMAN
PITTSBURGH, PA 15213

ENGINEERING SOCIETIES LIBRARY
ATTN ACQUISITIONS DEPT
345 EAST 47TH STREET
NEW YORK, NY 10017

IBM RESEARCH DIVISION
ALMADEN RESEARCH CENTER
ATTN R. M. MACFARLANE
MAIL STOP K32 802(D)
650 HARRY ROAD
SAN JOSE, CA 95120

JOHNS HOPKINS UNIVERSITY
DEPT OF PHYSICS
ATTN B. R. JUDD
BALTIMORE, MD 21218

KALAMAZOO COLLEGE
DEPT OF PHYSICS
ATTN K. RAJNAK
KALAMAZOO, MI 49007

DIRECTOR
LAWRENCE RADIATION LABORATORY
ATTN MARVIN J. WEBER
ATTN HELMUT A. KOEHLER
ATTN W. KRUPKE
LIVERMORE, CA 94550

MARTIN MARIETTA
ATTN F. CROWNE
ATTN R. LEAVITT
ATTN J. LITTLE
ATTN T. WORCHESKY
ATTN D. WORTMAN
1450 SOUTH ROLLING ROAD
BALTIMORE, MD 21227

MASSACHUSETTS INSTITUTE OF TECHNOLOGY
CRYSTAL PHYSICS LABORATORY
ATTN H. P. JENSSEN
ATTN A. LINZ
CAMBRIDGE, MA 02139

DISTRIBUTION (cont'd)

MASSACHUSETTS INSTITUTE OF TECHNOLOGY
77 MASS AVE
ROOM 26-251
ATTN V. BAGNATO
CAMBRIDGE, MA 02139

MIT LINCOLN LAB
PO BOX 73
ATTN PETER MOULTON,
ATTN B. AULL
LEXINGTON, MA 02173

DEPARTMENT OF MECHANICAL, INDUSTRIAL,
& AEROSPACE ENGINEERING
PO BOX 909
ATTN S. TEMKIN
PISCATAWAY, NJ 08854

NATIONAL OCEANIC & ATMOSPHERIC ADM
ENVIRONMENTAL RESEARCH LABS
ATTN LIBRARY, R-51, TECH RPTS
BOULDER, CO 80302

OAK RIDGE NATIONAL LABORATORY
ATTN R. G. HAIRE
OAK RIDGE, TN 37830

OKLAHOMA STATE UNIVERSITY
DEPT OF PHYSICS
ATTN R. C. POWELL (10 COPIES)
ATTN D. SARDAR (10 COPIES)
ATTN G. QUARLES (10 COPIES)
STILLWATER, OK 74078

PENNSYLVANIA STATE UNIVERSITY
MATERIALS RESEARCH LABORATORY
ATTN W. B. WHITE
ATTN B. K. CHANDRASEKHAR
UNIVERSITY PARK, PA 16802

SAN JOSE STATE UNIVERSITY
DEPARTMENT OF PHYSICS
ATTN J. B. GRUBER (3 COPIES)
SAN JOSE, CA 95192

SCIENCE APPLICATIONS, INC
ATTN T. ALLIK (20 COPIES)
ATTN SUSAN A. STEWART (10 COPIES)
1710 GOODRIDGE DRIVE
McCLEAN, VA 22102

SETON HALL UNIVERSITY
CHEMISTRY DEPARTMENT
ATTN H. BRITTAIN
SOUTH ORANGE, NJ 07099

PRINCETON UNIVERSITY
DEPARTMENT OF CHEMISTRY
ATTN D. S. McCLURE
PRINCETON, NJ 08544

UNIVERSITY OF MINNESOTA, DULUTH
DEPARTMENT OF CHEMISTRY
ATTN L. C. THOMPSON
DULUTH, MN 55812

UNIVERSITY OF VIRGINIA
DEPT OF CHEMISTRY
ATTN DR. F. S. RICHARDSON (2 COPIES)
ATTN DR. M. REID
CHARLOTTESVILLE, VA 22901

UNION CARBIDE CORP
ATTN M. R. KOKTA (10 COPIES)
ATTN J. H. W. LIAW
750 SOUTH 32ND STREET
WASHOUGAL, WA 98671

COMMANDER
NAVAL WEAPONS CENTER
ATTN CODE 3854, R. SCHWARTZ
ATTN CODE 3854, M. HILLS
ATTN CODE 3844, M. NADLER
ATTN CODE 385, R. L. ATKINS
ATTN CODE 343, TECHNICAL INFORMATION
DEPARTMENT
CHINA LAKE, CA 93555

AIR FORCE OFFICE OF SCIENTIFIC RESEARCH
ATTN MAJOR H. V. WINSOR, USAF
BOLLING AFB
WASHINGTON, DC 20332

US ARMY LABORATORIES COMMAND
ATTN COMMANDER, AMSLC-CG
ATTN TECHNICAL DIRECTOR, AMSLC-CT

INSTALLATION SUPPORT ACTIVITY
ATTN LEGAL OFFICE, SLCIS-CC
ATTN S. ELBAUM, SLCIS-CC

USAISC
ATTN RECORD COPY, ASNC-LAB-TS
ATTN TECHNICAL REPORTS BRANCH,
ASNC-LAB-TS (2 COPIES)

HARRY DIAMOND LABORATORIES
ATTN D/DIVISION DIRECTORS
ATTN LIBRARY, SLCHD-TL (3 COPIES)
ATTN LIBRARY, SLCHD-TL (WOODBRIDGE)
ATTN LIBRARY CHIEF, SLCHD-NW-E
ATTN CHIEF, SLCHD-NW-EP
ATTN CHIEF, SLCHD-NW-EH
ATTN CHIEF, SLCHD-NW-ES
ATTN CHIEF, SLCHD-NW-R
ATTN CHIEF, SLCHD-NW-TN
ATTN CHIEF, SLCHD-NW-RP
ATTN CHIEF, SLCHD-NW-CS
ATTN CHIEF, SLCHD-NW-TS
ATTN CHIEF, SLCHD-NW-RS
ATTN CHIEF, SLCHD-NW-P

DISTRIBUTION (cont'd)

HARRY DIAMOND LABORATORIES (cont'd)
ATTN CHIEF, SLCHD-PO
ATTN CHIEF, SLCHD-ST-C
ATTN CHIEF, SLCHD-ST-RS
ATTN CHIEF, SLCHD-ST-RA
ATTN CHIEF, SLCHD-TT
ATTN WALTER, SANDER, SLCIS-CP-TD
ATTN WILLIS, B., SLCHD-IT-EB
ATTN ZABLUDOWSKI, B., SLCHD-IT-EB
ATTN HERSHALL, P., SLCHD-MI-S
ATTN KENYON, C. S., SLCHD-NW-EP
ATTN MILETTA J. R., SLCHD-NW-EP
ATTN MCLEAN, F. B., SLCHD-NW-RP
ATTN SATTLER, J., SLCHD-PO-P
ATTN LIBELO, L., SLCHD-ST-MW
ATTN BENCIVENGA, A. A., SLCHD-ST-SP
ATTN NEMARICH, J., SLCHD-ST-SB
ATTN WEBER, B., SLCHD-ST-SB
ATTN BAHDER, T., SLCHD-ST-RP
ATTN BENCIVENGA, B. SLCHD-ST-AP
ATTN BRODY, P., SLCHD-ST-AP
ATTN BRUNO, J., SLCHD-ST-AP

HARRY DIAMOND LABORATORIES (cont'd)
ATTN DROPKIN, H., SLCHD-ST-AP
ATTN EDWARDS, SLCHD-ST-AP
ATTN HALL, K., SLCHD-ST-AP
ATTN HANSEN, A., SLCHD-ST-AP
ATTN HAY, G., SLCHD-ST-AP
ATTN KATZEN, E., SLCHD-ST-AP
ATTN NEIFELD, R., SLCHD-ST-AP
ATTN PENNISE, C., SLCHD-ST-AP
ATTN SCHMALBACH, R., SLCHD-ST-AP
ATTN SEMENDY, F., SLCHD-ST-AP
ATTN SIMONIS, G., SLCHD-ST-AP
ATTN SIMPSON, T., SLCHD-ST-AP
ATTN STEAD, M., SLCHD-ST-AP
ATTN STELLATO, J., SLCHD-ST-AP
ATTN TOBIN, M., SLCHD-ST-AP
ATTN TURNER, G., SLCHD-ST-AP (10 COPIES)
ATTN WONG, B., SLCHD-ST-AP
ATTN WORTMAN, D., SLCHD-ST-AP
ATTN GARVIN, C., SLCHD-ST-SS
ATTN GOFF, J., SLCHD-ST-SS
ATTN MORRISON, C., SLCHD-ST-AP (10 COPIES)


LMED
8